5th Joint International Symposium on Deformation Monitoring (JISDM), 20-22 June 2022, Valencia, Spain
DOI: http://doi.org/10.4995/JISDM2022.2022.13868

Comparison of TLS and sUAS point clouds for monitoring embankment dams

Dimitrios Bolkas[1], Matthew O'Banion[2], Jakeb Prickett[2], Gregory Ellsworth[1], Gerald Rusek[1], Hannah Corson[1]

[1] Department of Surveying Engineering, The Pennsylvania State University, Wilkes-Barre Campus, 44 University Drive, Dallas, PA 18612, USA, (dxb80@psu.edu; gje5059@psu.edu; gjr5221@psu.edu; hrc5135@psu.edu)
[2] Department of Geography & Environmental Engineering, United States Military Academy, 745 Brewerton Rd., West Point, NY 10996, USA, (matthew.obanion@westpoint.edu; jakeb.prickett@westpoint.edu)

Key words: *dam monitoring; terrestrial laser scanning; sUAS; accuracy assessment; point clouds*

ABSTRACT

Monitoring of dams is an essential surveying task to guarantee the safety of operation and understand the physical processes concerning their movement. Point cloud generating technologies are increasingly being utilized for monitoring of engineered structures. This paper compares point clouds acquired from terrestrial laser scanning (TLS) and small unmanned aerial systems (sUAS)-based photogrammetry for monitoring of the Francis E. Walter dam in northeast Pennsylvania. Authorized for construction by the Flood Control Act of 1946, and with renewed interest due to extensive flooding in 1955 caused by the back-to-back hurricanes Connie and Diane, this earth-filled embankment dam was completed in June of 1961 by the U.S. Army Corps of Engineers. It is currently operated in conjunction with Beltzville Lake for stage reductions on the Lehigh River. The dam is being monitored through conventional surveying methods (total station) every five years. In spring of 2021 a TLS and sUAS data acquisition took place to assess the feasibility and utility of using modern point cloud technologies for monitoring. This paper presents a comprehensive comparison and accuracy assessment of the two point cloud collection methods, considering several parameters for the generation of the sUAS photogrammetric point cloud. Results show the advantages and disadvantages of the two methods. For instance, TLS offers high accuracy (cm-level), but suffers from data gaps due to line of sight blockage/occlusion. On the other hand, sUAS photogrammetry offers more complete point clouds, but presents more challenges in georeferencing and in the generation of accurate point clouds. Similar insights and lessons learned are useful for future surveying tasks and monitoring of similar embankment dam structures.

I. INTRODUCTION

Periodic and frequent monitoring of engineering structures is important for ensuring their integrity and guarantee their safety of operation (Scaioni *et al.*, 2018). Surveying methods have long been used to monitor engineering structures such as dams to monitor and understand the physical processes concerning their movement. While traditional surveying methods, using total station instruments and/or global navigation satellite system (GNSS) observations, have been proven accurate and reliable (Jeon *et al.*, 2009; Xi *et al.*, 2018; Xiao *et al.*, 2019) they do pose limitations. For instance, they require lengthy data acquisition durations which limits the number of discrete points that can be monitored. To address the issue of long data acquisitions, permanent robotic total stations and GNSS receivers are being installed for monitoring dams in frequent intervals or near-real time. Ground based synthetic aperture radar (GBSAR) is a technology that can provide measurements at the ± 1 mm level and can be used to capture displacement patterns in high spatial resolution than just at a few discrete points. In its continuous mode of operation, the unit needs to be installed permanently (Alba *et al.*, 2008; Scaioni *et al.*, 2018), and its discontinuous mode necessitates revisiting the site periodically (Alba *et al.*, 2006; Mascolo *et al.*, 2014), which can introduce challenges in phase ambiguity estimations. Furthermore, displacements are given along the line of sight and not in 3D coordinates (Scaioni *et al.*, 2018).

On the other hand, point cloud technologies from terrestrial laser scanning (TLS) are gaining ground as they offer high spatial resolution with accuracies around ±1–2 cm (Mukupa *et al.*, 2017); however, this also depends on the registration approach. When monitoring concrete dams, deformation levels are observed at the mm-level (Scaioni *et al.*, 2018), making TLS monitoring a challenging task. In this case rigorous estimation of TLS errors and error propagation is necessary to distinguish between noise and deformation (Mukupa *et al.*, 2017; Scaioni *et al.*, 2018; Li *et al.*, 2021). In addition, in concrete dams TLS can take advantage of their physical shape and fit a parametric surface on the point cloud such as polynomial surface (Alba *et al.*, 2006) or radial basis functions (González-Aguilera *et al.*, 2008). TLS is more appropriate for monitoring earth-rock embankment

dams, due to the higher magnitude tolerated, which can be at the few cm- to dm-level (Xu *et al.*, 2019).

Recently small unmanned aerial system (sUAS) photogrammetry has been used to monitor dams with accuracies on the order of a few cm-level (e.g., Buffi *et al.*, 2017; Ridolfi *et al.*, 2017; Khaloo *et al.*, 2018; Zhao *et al.*, 2021); therefore, making this technology more suitable for monitoring earth-rock dams. For concrete dams, use of sUAS is better suited for inspection of the dam structure and identification of cracks (Zhao *et al.*, 2021). Despite the lower accuracy of sUAS photogrammetry compared to TLS, the technology offers some advantages such as an improved vantage point and a less obscured line of sight when compared to many perspectives (*e.g.*, O'Banion *et al.*, 2018; Bolkas *et al.*, 2021). In general, sUAS and TLS methods also provide a relatively fast data acquisition solution that results in the generation of a dense point cloud dataset. The major drawback is that sUAS and TLS methods often need an extensive network of control points for georeferencing.

Considering the differences in the TLS and sUAS technologies, this paper makes a comparison of TLS and sUAS derived point clouds for monitoring earth-filled embankment dams. The Francis E. Walter Dam that is being investigated in this paper, has been monitored with traditional total station methods. The paper provides a comprehensive analysis of TLS and sUAS methods and discusses their potential for continued monitoring of this site in the following years.

II. Study Area and Datasets

A. *Francis E. Walter dam*

The Francis E. Walter dam is located in northeast Pennsylvania approximately 7 km northeast from the town of White Haven, PA. It is an earth-filled embankment dam that was completed in 1961 by the U.S. Army Corps of Engineers (U.S. Army Corps of Engineers 2021). The dam represents a flood control project and is currently operated in conjunction with Beltzville Lake for stage reductions on the Lehigh River. The dam is also a popular recreation destination for fishing, boating, and various paddle sports. The dam has prevented over $296 million in cumulative damages between 1961 and 2021. The dam has a maximum length of about 910 m, a height of 71 m (foundation to crest), and a base width of 370 m. The capacity of the dam's reservoir is 0.1365 km^3, and its drainage catchment area is around 750 km^2.

The embankment is composed of essentially six different types of material. The central core is composed of an impervious fill that extends into the embankment foundation. In addition, a blanket of impervious fill has been placed along the foundation on the upstream side of this core. Above, and upstream of the central core, is a zone of pervious fill. Adjacent to the downstream side of the core, and along the downstream foundation, is a thin layer of pervious material. Downstream, and above this thin layer is a zone of non-engineered fill. Around the entirely exposed periphery of the embankment, except for the 9 m wide top and downstream toe, there is a protective layer of riprap. The downstream toe of the embankment, in a vertical direction, is composed of rock, impervious fill and non-engineered fill. The top of the dam is 9 m wide at an elevation of 449 m. The last major Lehigh River Basin flood occurred in June of 2006 and resulted in a record pool elevation of 439 m.

B. *Control network*

To support the TLS and sUAS data acquisitions a network of 27 points was created. Two control points about one kilometer away from the dam were used as stable references. Some of the 27 points are pre-existing monument disks, some are drill holes in bedrock, mag nails driven into asphalt, and sensor pins (Figure 1). A rapid static Global Navigation Satellite System (GNSS) network was created with at least of 15 minutes of common occupation between baselines. The post adjustment standard deviations were at the 2-3 mm-level, which reflects the internal consistency of the network. With consideration of centering errors, it is estimated that positional accuracy of the control network is at the ±1 cm level, which is sufficient for supporting the TLS and sUAS surveys.

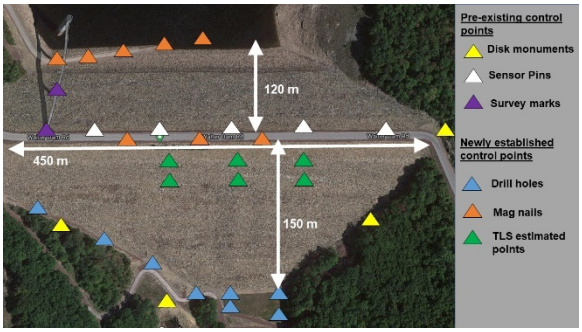

Figure 1. Overview of Francis E. Walter dam and control points for the TLS and sUAS surveys. Dimensions shown are length (450 m) and width (150 m and 120 m). Background image from Google Maps.

C. *TLS survey*

A Leica Scan Station P50 was used for the TLS survey (instrument specifications are presented in Table 1). The P50 is a panoramic scanner that offers fast scan rates allowing for fast data acquisition. Its range and angular accuracies are high, ensuring point clouds that are high in accuracy and quality.

The scanning resolution was set to 2 cm at a range of 120 m. Maximum scanning range was set to 120 m, as points can be captured with as little as 8% reflectivity. At a range of 270 m, minimum target reflectivity is significantly higher at 34%. This decrease in sensor sensitivity in conjunction with any registration and measurement errors can lead to higher overall errors in the point cloud. Therefore, it was decided to decrease

the maximum range and increase the number of TLS station setups, which also helps to reduce data gaps due to line of sight obstructions.

Table 1. Leica Scan Station P50 technical specifications information were retrieved from: Leica Geosystems (2021)

Technical specifications	Value
Range accuracy	1.2 mm + 10 ppm
Angular accuracy	8" horizontal; 8" vertical
Dual-axis compensator	Resolution 1", dynamic range ±5', accuracy 1.5"
Beam diameter at front window and beam divergence	3.5 mm, 0.23 mrad Full width at half maximum
Scan rate	1,000,000 points per second

Data collection took place one week after the establishment of the GNSS network on March 21, 2021. Multiple scans were acquired from the base and crest of the dam. The previously discussed control network was used to register the numerous TLS scans. The method of resection was chosen to increase redundancy and derive standard deviations for the estimation of registration accuracy. In most cases at least three control points were used for the resection, except for cases where a third control point was not in view. A resection estimation of only four parameters (three translations and one rotation around the z-axis) was necessary given the use of the P50's accurate onboard dual-axis tilt compensator. Standard deviations for resection did not exceed ± 1 cm for each coordinate component (easting, northing, elevation).

D. *sUAS survey*

sUAS data were collected on April 13, 2021, about 20 days after the TLS data collection due to bad weather and higher winds throughout the region. At the time of the sUAS data collection, the reservoir water level was higher and for safety reasons only the protected side was surveyed.

The sUAS survey was completed using an Aibotix sUAS carrying a Sony α6000 mirrorless digital camera. The digital camera has a 24-megapixel imaging sensor. Aerial images were taken with a 16 mm focal length and a 1/2,000 second shutter speed. The sUAS payload includes a GNSS- Real Time Kinematic (RTK) antenna, allowing for cm level positioning when a base station is used. A GNSS base station was setup at the base of the downstream side of the dam.

Two flights were conducted covering a smaller region than the TLS survey (see Table 2 and Figures 2 and 3). The two flights followed different patterns. The first flight was conducted at a fixed altitude of around 110 m above ground at the base of the dam on the downstream side, which reduced to about 50 m above ground level at the crest of the dam. The orientation of this flight was perpendicular to the road as shown in Figure 3d. A total of 10 flight lines were used, and 156 images were captured. Image endlap was 85%, with 85% sidelap reduced to 60% at the crest. For the second flight, flight line orientation was parallel to the road and the altitude changed for each flight line to maintain more constant heights above ground. A total of five flight lines were used and 190 images were captured. Flying heights remained constant around 60 m except for the last flight line at the dam crest that was closer 50 m above ground level. Image endlap was 85% and 75% sidelap, which reduced to about 60% for the last flight line at the crest of the dam. The resulting average ground sample density (GSD) of the point cloud for the across flight is 4 cm., and the average GSD of the point cloud for the parallel flight is 3 cm. The average GSD are a result of the trade-offs and limitations of the available sUAS and resources for this project.

Table 2. sUAS flight characteristics for April 2021

Parameter	Across flight	Parallel flight
Altitude [m]	50 to 110	60 (50 for last flight line at crest)
Flightlines	10	5
Images	156	190
Endlap	85%	85%
Sidelap	60% to 85%	75% (60% for last flight line at crest)
GSD [cm]	4	3

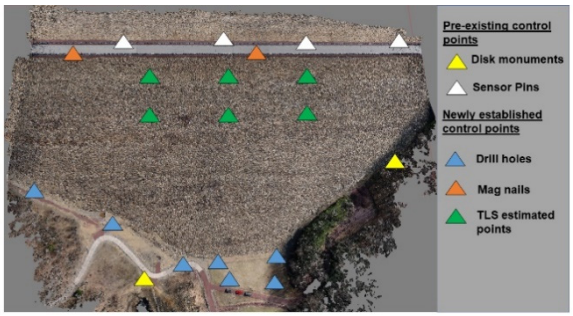

Figure 2. Control points used by the sUAS flights and sUAS point cloud using both the Across and Parallel flights.

Agisoft Metashape was used for photogrammetric processing of the sUAS images. Of the 27 control points, 14 control points were in view. To comply with the United States Federal Aviation Administration (FAA) regulations, the sUAS remained a minimum of 20 m from the roadway located on the crest of the dam. This offset resulted in two control points being hidden from view due to the location of the roadway guardrail relative to the sUAS perspective. Control point coverage was adequate at the base and crest of the dam; however, no control points were set on the downstream face of the dam due to safety concerns associated with traversing the riprap. To augment georeferencing and reduce control network gaps, we extracted six control points from the TLS point cloud. These control points represent corners on piezometer boxes that were well captured in the TLS survey. Three planes were fitted using random sample consensus

(RANSAC) and their intersection was used to estimate a corner point. Thus, a total of 20 control points were used. In addition, six points along the guardrail were also extracted to serve as checkpoints.

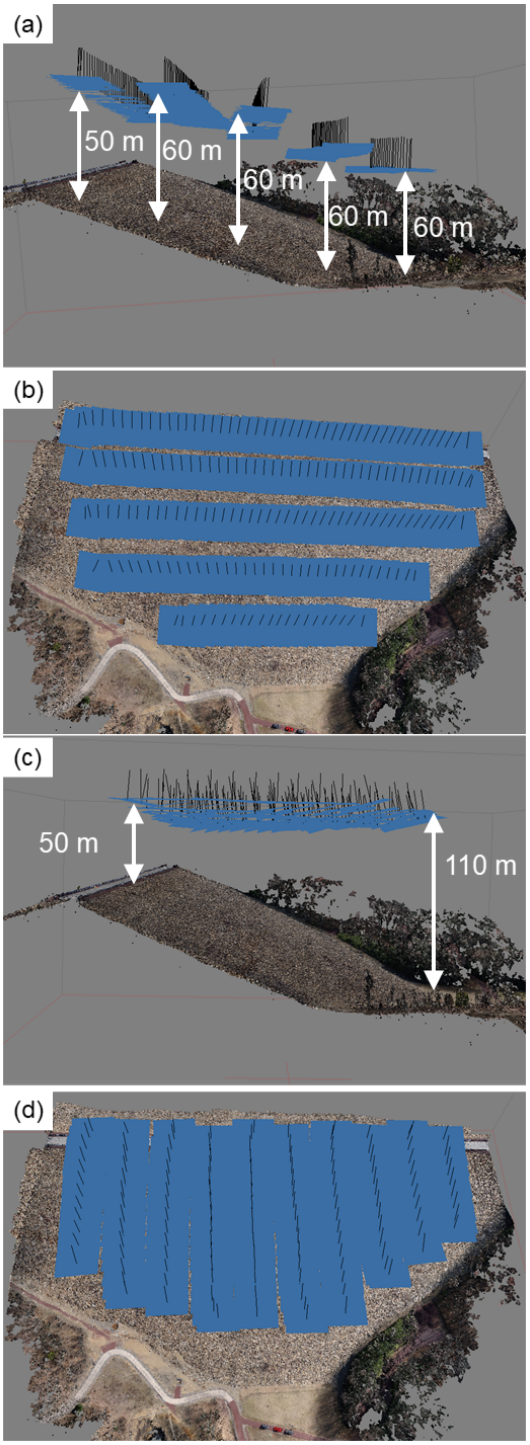

Figure 3. sUAS flights, (a) and (b) show the flight lines that run parallel to the Francis E. Walter dam road, and (c) and (d) show the flight lines that run perpendicular to the Francis E. Walter dam road.

Based on previous experience with the AiBotix sUAS, 4 to 6 control points are known to be sufficient for achieving cm-level georeferencing accuracy (Bolkas, 2019), but this conclusion was based on smaller sites of about 5.5 acres in size.

III. Results

A. *Data acquisition discussion*

Before going into the accuracy comparison of the two methodologies, we compare and discuss the data acquisition process, safety, and completeness of the data. With respect to time spent in the field, about two days (16 hours of work) were needed to capture the TLS point clouds on both sides of the dam. For the sUAS surveys, the biggest constraint was the common occurrence of high-speed winds in the region. Wind strength often increases throughout the dam site after 10 am, resulting in a narrow window that is suitable for sUAS operation. The manufacturer of the Aibotrix sUAS recommends that flights should not be conducted when winds exceed 8 m/s. In addition, the increased reservoir water level observed in April flooded the access roads on the upstream side of the dam, which forced the cancelation of the upstream flight due to absence of an adequate takeoff and landing site and access issues.

Despite the many TLS station setups, the resulting point cloud had several data gaps at the half meter level due to line-of-sight obstructions. Figure 4 shows data gaps in the TLS dataset, which for the most part are around 0.5 m, except for some areas where line of sight was significantly blocked leading to gaps of about 2.0 m. On the other hand, sUAS surveys generated a more consistent point cloud devoid of any large data gaps, as it offers a more unobstructed view of the dam. This shows how the two technologies have different advantages and disadvantages, which should be considered before deciding which technology is preferable. In the next paragraphs we discuss the accuracy comparison between the two surveying methods.

B. *Comparison of sUAS Photogrammetry and TLS*

A significant challenge in estimating deformations using point clouds is that the available technologies do not survey the exact same point over time (Mukupa *et al.*, 2017). The estimation of differences between multi-epoch point clouds is often implemented using the model-to-model cloud comparison (M3C2) algorithm (Lague *et al.*, 2013), which allows for robust cloud-to-cloud comparison. This approach was followed here to estimate the difference between the TLS and the sUAS point clouds.

We found that when using the TLS datasets as the reference, RMSE values were considerably higher than they should be (at the 20 cm level). We attribute this to the data gaps present in the TLS data and the TLS core points that are generated in the M3C2 distance calculation. In addition, we had to restrict the projection and normal diameter in the M3C2 distance calculations to 25 cm, otherwise distances had a bias of up to 8 cm. This can also be attributed to the TLS point cloud data gaps, as larger projections and diameters would increase the chance of including data gap regions in the distance calculation. Table 3 shows the first order

statistics, mean and standard deviation (SD), using the sUAS datasets as the reference. The table shows a high level of agreement between the sUAS and TLS point clouds with almost zero mean values and SD values at the 3.3 to 3.6 cm level. The across flight is slightly better than the parallel flight, as the latter had some higher errors in the top left side of the study site. The combined dataset shows a mean value of 0.1 cm and SD of 3.3 cm, indicating a strong agreement between the two datasets. The analysis in this section shows that despite the different flight pattern, similar sUAS point clouds were retrieved, especially for the across flight, where a fixed flying height was followed, and therefore distance from the ground was variable because of the dam slope.

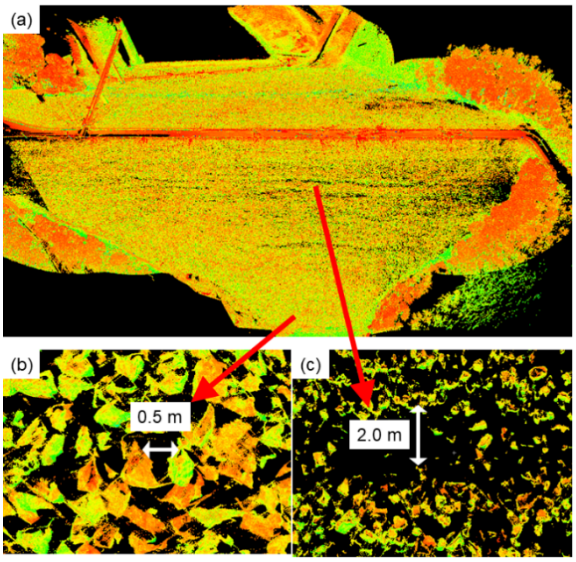

Figure 4. TLS point cloud and data gaps resulting from line-of-sight obstructions.

Table 3. Mean and SD values for various scenarios. All sUAS datasets are processed with Agisoft Metashape

Comparison	Mean [cm]	SD [cm]
sUAS Across vs TLS	0.1	3.3
sUAS Parallel vs TLS	0.4	3.6
sUAS Combined vs TLS	0.1	3.3
sUAS Across vs sUAS Parallel	0.0	3.0

Figure 5 shows the histogram based on the M3C2 distances between the sUAS point clouds and the TLS point cloud, while Figure 6 shows a spatial visualization of the M3C2 distances. Both the across and parallel sUAS point clouds have a similar histogram shape, with the across flight having a slightly higher peak. The spatial visualization of the M3C2 distances shows that the parallel flight has some higher error in the left side of the dam, which are due to misalignment of the photos. In the parallel flight two of the leftmost control points shown in Figure 2 were only visible from two images each, decreasing alignment accuracy.

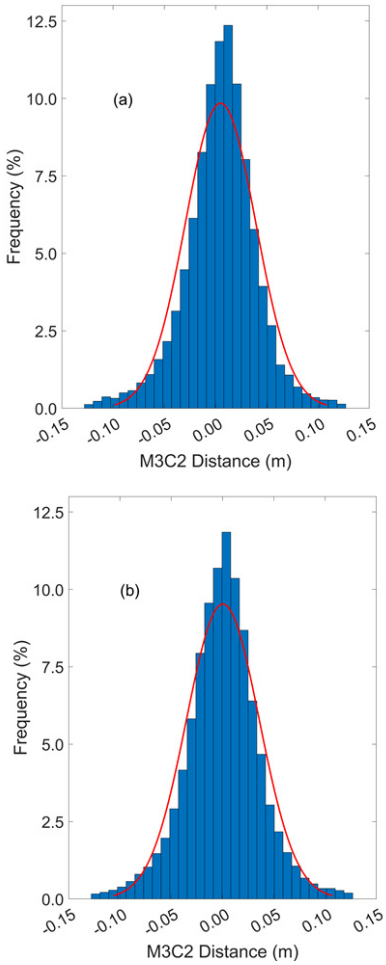

Figure 5. Histograms based on the M3C2 distance: (a) sUAS Across flight vs TLS, mean of 0.1 cm, and SD of 3.3 cm; (b) sUAS parallel flight vs TLS mean of 0.4 cm, and SD of 3.6 cm.

Assuming that the TLS dataset has an accuracy at the ±1-1.5 cm level, then the estimated accuracy of the sUAS point cloud is about ±2.9 cm to ±3.1 cm. This is considered reasonable, considering the average GSD of 3.0 cm for the photogrammetric point cloud. The U.S. Army Corps of Engineers accuracy requirements for performing deformation surveys state that for each survey, final positioning accuracy (at the 95% confidence level), should be less or equal to one-fourth of the predicted (maximum) displacement (U.S. Army Corps of Engineers, 2009). This indicates that the present sUAS point clouds can be used to detect displacements of 23 cm – 24.6 cm or greater. Normal vertical settlement of earth-filled embankment dams is at the level of 40.0 cm over 5-10 years during the stabilizing phase (U.S. Army Corps of Engineers, 2009). Therefore, photogrammetric methods with resulting accuracy at the ±3-4 cm level, can be used for monitoring comparison over 5–10-year intervals; however, a greater accuracy at the level of ±1-2 cm is needed for year-to-year comparisons. Such accuracies are easier met by TLS methods. Another approach is to upgrade the sUAS system, *e.g.*, upgrading the sUAS camera, from 24 megapixels to 40 megapixels in our case, which would result in a higher GSD. Indeed, this

will be our future approach to enhance our assessment of earth-filled embankment dams using sUAS methods and assess monitoring for shorter periods of time.

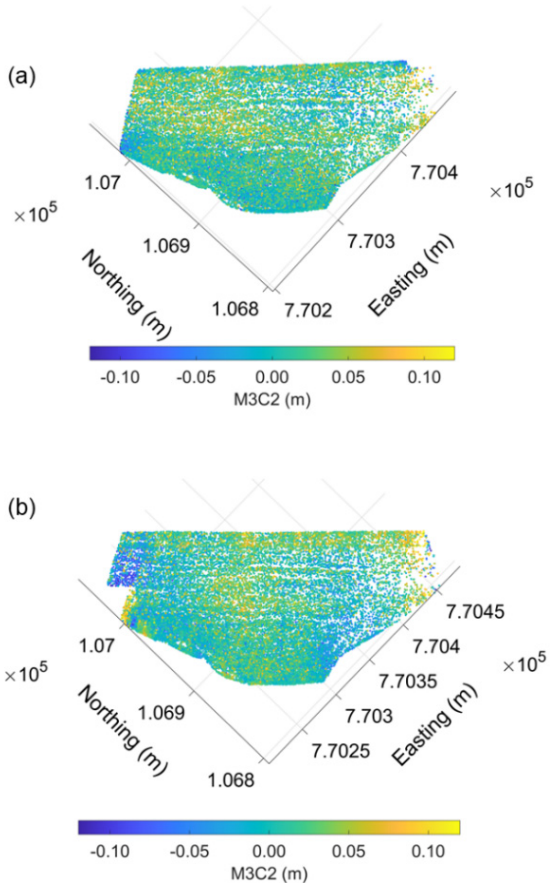

Figure 6. Spatial visualization of M3C2 distances: (a) sUAS Across flight vs TLS, mean of 0.1 cm, and SD of 3.3 cm; (b) sUAS parallel flight vs TLS mean of 0.4 cm, and SD of 3.6 cm.

C. *Comparison of photogrammetry software*

We processed the sUAS images with both Agisoft Metashape and Leica Infinity software and found that the Metashpe point cloud to be more accurate. The Leica Infinity dataset has a mean value of 1.3 cm, which indicates the presence of a small bias, and a higher SD of 4.3 cm (Table 4). The histogram comparison in Figure 7 shows a higher peak of the sUAS point cloud when processed with Agisoft Metashape than the Leica Infinity. In addition, Figure 7a shows that most differences between the TLS and the sUAS point cloud are within a range of ± 10 cm.

A spatial visualization of the M3C2 distances is shown in Figure 8. Figure 8a indicates that lower errors exist in the middle of the dam. Higher (positive) errors existing at the right of the dam, which can be attributed to the larger data gaps in the TLS dataset. Also, high (negative) errors exist in the left side of the dam in Figure 8a, indicating a small misalignment error. In the same left side of the dam, higher errors (positive) are found for the Leica Infinity point cloud in Figure 8b, suggesting a bigger misalignment issue. On this side of the dam not all control points were visible, as a couple of the control points on the left side of the main road where hidden by the guard-rail in some images and only visible in 2-3 images. The field crew did not want to fly close to the road for safety and this issue was not noticed until the images were processed. Therefore, better flight planning in the future would be able to address this issue and provide an even more accurate sUAS point cloud.

Table 4. Mean and SD values for scenarios of Agisoft Metashape versus Leica Infinity

Comparison	Mean [cm]	SD [cm]
sUAS Combined (Agisoft) vs TL	0.1	3.3
sUAS Combined (Infinity) vs TLS	1.3	4.3
sUAS combined (Infinity) vs sUAS Combined (Agisoft)	0.0	4.4

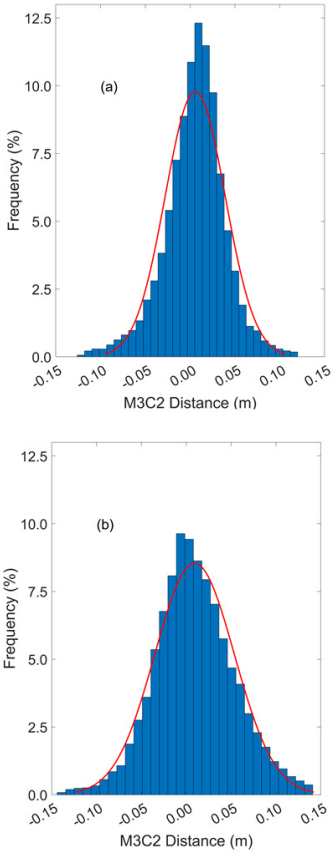

Figure 7. Histograms based on the M3C2 distance: (a) sUAS Combined (Agisoft) vs TLS, mean of 0.1 cm, and SD of 3.3 cm; (b) sUAS Combined (Infinity) vs TLS mean of 1.3 cm, and SD of 4.3 cm.

IV. Conclusions

Monitoring of engineering structures such as bridges, dams, levees, etc., is important for ensuring their integrity and safety of operation. This paper presented an evaluation and comparison of sUAS photogrammetry and TLS technologies at the Francis E. Walter Dam in northeast Pennsylvania. The network of control points was expanded to accommodate the registration of TLS stations through resection and the georeferencing of sUAS photogrammetric data. Datasets presented here were from the same epoch.

The accuracy assessment indicates that the TLS data is consistent to within ± 1 cm, and the sUAS derived data aligns with TLS data at the ± 3.3 cm level. The TLS accuracy levels of accuracy are considered sufficient for year-to-year monitoring of earth-filled embankment dams where smaller displacements are expected (*e.g.*, 5.0 - 14.0 cm per year), while the sUAS accuracy level is more suitable for 5–10-year intervals where larger displacements are expected (*e.g.*, about 40.0 cm).

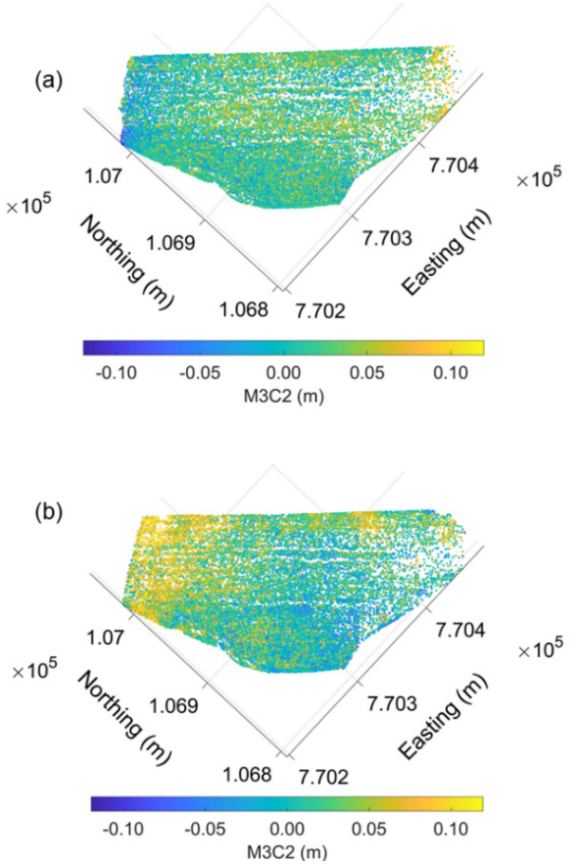

Figure 8. Spatial visualization of M3C2 distances: (a) sUAS Combined (Agisoft) vs TLS, mean of 0.1 cm, and SD of 3.3 cm; (b) sUAS Combined (Infinity) vs TLS mean of 1.3 cm, and SD of 4.3 cm.

Future work will entail the use of a sUAS that includes a higher resolution 42-megapixel digital camera, an onboard post-processed kinematic (PPK) GNSS receiver, and the ability to safely fly in higher speed winds. This will allow us to assess the capacity and extend of sUAS photogrammetry to monitor displacement in shorter periods of time. Hence, monitoring of the site will continue with the same sensors in the following years (with one dataset every year) to create a multi-epoch and multi-platform time lapse. The existence of data gaps in the TLS dataset can introduce challenges in estimating multi-epoch differences. Therefore, another future goal will be on developing an algorithm for robust estimation of multi-epoch differences for similar earth-rock dams.

V. Acknowledgements

This project has received funding from Chancellor Endowment Funds, Penn State University, Wilkes-Barre Campus. The authors would like to acknowledge David Williams and Brett Anderton, U.S. Army Corps of Engineers, for their assistance in this project. In addition, undergraduate student Nick Lawler is thanked for his contribution in the data collection.

References

Alba, M., Fregonese, L., Prandi, F., Scaioni, M., and Valgoi, P. (2006). Structural monitoring of a large dam by terrestrial laser scanning. *International Archives of Photogrammetry, Remote Sensing and Spatial Information Sciences*, Vol. 36, No. 5, pp. 6.

Alba, M., Bernardini, G., Giussani, A., Ricci, P. P., Roncoroni, F., Scaioni, M., Valgoi P., and Zhang, K. (2008). Measurement of dam deformations by terrestrial interferometric techniques. *International Archives of Photogrammetry, Remote Sensing and Spatial Information Sciences*, Vol. 37, No. B1, pp. 133-139.

Bolkas, D. (2019). Assessment of GCP number and separation distance for small UAS surveys with and without GNSS-PPK positioning. *Journal of Surveying Engineering*, Vol. 145, No. 3, pp. 04019007.

Bolkas, D., Walton, G., Kromer, R., and Sichler, T. (2021). Registration of multi-platform point clouds using edge detection for rockfall monitoring. *ISPRS Journal of Photogrammetry and Remote Sensing*, Vol. 175, pp. 366-385.

Buffi, G., Manciola, P., Grassi, S., Barberini, M., and Gambi, A. (2017). Survey of the Ridracoli Dam: UAV–based photogrammetry and traditional topographic techniques in the inspection of vertical structures. *Geomatics, natural hazards and risk*, Vol. 8, No. 2, pp. 1562-1579.

González-Aguilera, D., Gómez-Lahoz, J., and Sánchez, J. (2008). A new approach for structural monitoring of large dams with a three-dimensional laser scanner. *Sensors*, Vol. 8, No. 9, pp. 5866-5883.

Jeon, J., Lee, J., Shin, D., and Park, H. (2009). Development of dam safety management system. *Advances in Engineering Software*, Vol. 40, No. 8, pp. 554-563.

Khaloo, A., Lattanzi, D., Jachimowicz, A., and Devaney, C. (2018). Utilizing UAV and 3D computer vision for visual inspection of a large gravity dam. *Frontiers in Built Environment*, Vol. 4, No. 31.

Lague, D., Brodu, N., and Leroux, J. (2013). Accurate 3D comparison of complex topography with terrestrial laser scanner: Application to the Rangitikei canyon (NZ). *ISPRS Journal of Photogrammetry and Remote Sensing*, Vol. 82, pp. 10-26.

Leica Geosystems (2021). Leica ScanStation P50 – Long Range 3D Terrestrial Laser Scanner. Accessed online on November 30, 2021: https://leica-geosystems.com/en-us/products/laser-scanners/scanners/leica-scanstation-p50

Li, Y., Liu, P., Li, H., and Huang, F. (2021). A Comparison Method for 3D Laser Point Clouds in Displacement Change Detection for Arch Dams. *ISPRS International Journal of Geo-Information*, Vol. 10, No. 3, pp. 184.

Mascolo, L., Nico, G., Di Pasquale, A., and Pitullo, A. (2014). Use of advanced SAR monitoring techniques for the assessment of the behaviour of old embankment dams. In: *Proc of Earth Resources and Environmental Remote Sensing/GIS Applications V*, Vol. 9245, p. 92450N. International Society for Optics and Photonics.

Mukupa, W., Roberts, G. W., Hancock, C. M., and Al-Manasir, K. (2017). A review of the use of terrestrial laser scanning application for change detection and deformation monitoring of structures. *Survey review*, Vol. 49, No. 353, pp. 99-116.

O'Banion, M.S., Olsen, M.J., Rault, C., Wartman, J., Cunningham, K. (2018). *Suitability of Structure from Motion for Rock Slope Assessment.* The Photogrammetric Record, Vol. 33, No. 162, pp. 217-242.

Ridolfi, E., Buffi, G., Venturi, S., and Manciola, P. (2017). Accuracy analysis of a dam model from drone surveys. *Sensors*, Vol. 17, No. 8, pp. 1777.

Scaioni, M., Marsella, M., Crosetto, M., Tornatore, V., and Wang, J. (2018). Geodetic and remote-sensing sensors for dam deformation monitoring. *Sensors*, Vol. 18, No. 11, pp. 3682.

U.S. Army Corps of Engineers (2009) *Engineering and Design: Structural Deformation Surveying*. Department of the Army, U.S. Army Corps of Engineers, Washington, DC, Manual No. 1110-2-1009.

U.S. Army Corps of Engineers (2021). Francis E. Walter Dam. https://www.nap.usace.army.mil/Missions/Civil-Works/Francis-E-Walter-Dam/ [Accessed November 11 202

Xi, R., Zhou, X., Jiang, W., and Chen, Q. (2018). Simultaneous estimation of dam displacements and reservoir level variation from GPS measurements. *Measurement*, Vol. 122, pp. 247-256.

Xiao, R., Shi, H., He, X., Li, Z., Jia, D., and Yang, Z. (2019). Deformation monitoring of reservoir dams using GNSS: an application to south-to-north water diversion project, China. *IEEE Access*, Vol. 7, pp. 54981-54992.

Xu, H., Li, H., Yang, X., Qi, S., and Zhou, J. (2019). Integration of terrestrial laser scanning and nurbs modeling for the deformation monitoring of an earth-rock dam. *Sensors*, Vol. 19, No. 1, pp. 22.

Zhao, S., Kang, F., Li, J., and Ma, C. (2021). Structural health monitoring and inspection of dams based on UAV photogrammetry with image 3D reconstruction. *Automation in Construction*, Vol. 130, pp. 103832.